Natural sesquiterpene lactones as inhibitors of Myb-dependent gene expression: Structure-activity relationships

ARTICLE *in* EUROPEAN JOURNAL OF MEDICINAL CHEMISTRY · FEBRUARY 2013

Impact Factor: 3.45 · DOI: 10.1016/j.ejmech.2013.02.018 · Source: PubMed

5 AUTHORS, INCLUDING:

Fernando Batista Da Costa
University of São Paulo
95 PUBLICATIONS **1,272** CITATIONS
SEE PROFILE

Karl-Heinz Klempnauer
University of Münster
115 PUBLICATIONS **5,241** CITATIONS
SEE PROFILE

Thomas J. Schmidt
University of Münster
142 PUBLICATIONS **2,900** CITATIONS
SEE PROFILE

European Journal of Medicinal Chemistry 63 (2013) 313–320

Contents lists available at SciVerse ScienceDirect

European Journal of Medicinal Chemistry

journal homepage: http://www.elsevier.com/locate/ejmech

Original article

Natural sesquiterpene lactones as inhibitors of Myb-dependent gene expression: Structure–activity relationships

Caroline Schomburg [a,1], Wolfgang Schuehly [b], Fernando B. Da Costa [c], Karl-Heinz Klempnauer [d], Thomas J. Schmidt [a,*]

[a] Institute of Pharmaceutical Biology and Phytochemistry (IPBP), University of Münster, Hittorfstr. 56, D-48149 Münster, Germany
[b] Department of Pharmacognosy, Institute of Pharmaceutical Sciences, Karl-Franzens-University Graz, Universitätsplatz 1, 8010 Graz, Austria
[c] School of Pharmaceutical Sciences of Ribeirão Preto (FCFRP), University of São Paulo (USP), Av. do Café s/no., 14040-903 Ribeirão Preto, SP, Brazil
[d] Institute of Biochemistry, University of Münster, Wilhelm-Klemm-Str. 2, D-48149 Münster, Germany

ARTICLE INFO

Article history:
Received 5 November 2012
Received in revised form
12 February 2013
Accepted 15 February 2013
Available online 26 February 2013

Keywords:
Sesquiterpene lactone
Anticancer
c-Myb
Structure–activity relationship
Pharmacophore
QSAR

ABSTRACT

c-*myb* is a proto-oncogene encoding a transcription factor which is highly expressed in hematopoietic progenitor cells. It regulates the expression of genes important for lineage determination, cell proliferation, and differentiation. Deregulation of c-*myb* expression is known to be involved in the development of human tumors, especially certain types of leukemia and breast and colon cancer. The c-Myb protein has thus been identified as an interesting therapeutic target. We recently discovered that some sesquiterpene lactones suppress Myb-dependent gene expression which is a new mechanism for these natural products' potential anti-cancer activity. We developed a test system to screen compounds for inhibitory activity on Myb-inducible reporter gene activation. Using this system we have now investigated 60 sesquiterpene lactones for their capacity to inhibit c-Myb-dependent gene activation. The IC_{50} values were in a range between 0.7 and >30 μM. The furanoheliangolide goyazensolide and the pseudoguaianolide helenalin acetate (IC_{50} = 0.6 and 0.7 μM, respectively) represent the most active inhibitors of c-Myb dependent gene expression found up to present. Control measurements for cell viability (MTS assay) proved that the observed activity on c-Myb dependent gene expression is not a function of cytotoxicity/unspecific cell damage.

Structure–activity relationships were investigated by a QSAR approach based on flexible alignment of the most active compounds and a common pharmacophore model. These investigations resulted in a QSAR model which indicates that the potency of inhibitory activity on c-Myb-dependent transcription does not only depend on the presence of reactive Michael-acceptor features but also on their optimal spatial arrangement in the molecule.

1. Introduction

Proto-oncogenes of the *myb*-family (A-*myb*, B-*myb*, and c-*myb*), encode transcription factors that regulate the expression of genes with important functions for lineage determination, cell proliferation, and differentiation [1–4]. The c-*myb* gene is expressed predominantly in the hematopoietic system and has been demonstrated in various studies to play a crucial role in the development of most lineages of this system [5–10]. Its expression is highest in the immature progenitors of all hematopoietic lineages. Down-regulation of *c-myb* is known to be essential for their terminal differentiation. Furthermore, *c-myb* is also expressed in some other tissues [11] where it plays a role, e.g., in the proliferation of colonic crypt progenitor cells [12].

The protein encoded by c-*myb* (c-Myb) is a transcription factor which regulates the expression of a large variety of genes, including genes involved in proliferation, cell survival and differentiation [13–16]. Furthermore, strong evidence has been presented that its deregulation plays a role in the development of certain leukemias and of breast and colon tumors. It has hence been suggested that suppression of c-Myb-induced gene activation might be a valuable therapeutic strategy [4].

In a recent communication, we demonstrated that some natural sesquiterpene lactones (STLs) isolated from plants of the Sunflower family (Asteraceae) are able to inhibit the activation of Myb-inducible genes [17]. We developed a fluorescence-based assay system that allows screening of compounds for their ability to suppress the activation of a Myb-inducible reporter gene. This system has now

* Corresponding author. Tel.: +49 251 83 33378; fax: +49 251 83 38341.
E-mail address: thomschm@uni-muenster.de (T.J. Schmidt).
[1] Part of current doctoral thesis.

0223-5234/$ – see front matter © 2013 Elsevier Masson SAS. All rights reserved.
http://dx.doi.org/10.1016/j.ejmech.2013.02.018

been used to screen a series of 60 natural STLs for their potency in inhibiting c-Myb activity and, on this basis, to study structure–activity relationships for this first group of soluble low-molecular weight Myb inhibitors using complementary *in silico* approaches.

2. Results and discussion

2.1. Differential inhibitory activity of sesquiterpene lactones on c-Myb dependent gene expression

We have recently developed a stable reporter cell line in which a doxycyclin-inducible expression system for c-Myb was combined with an eGFP reporter gene driven by the promoter and enhancer of the Myb-responsive chicken *mim-1* gene [17]. When Myb expression is induced by doxycyclin in these cells, the increase in fluorescence intensity can be used as a read-out for Myb activity. We have now used this reporter cell line to investigate the inhibitory activity of 60 natural STLs on the ability of c-Myb to stimulate the transcription of the reporter gene. The structures and activity data of the tested compounds are reported in Fig. 1 and Table 1.

Quite noteworthy, two compounds belonging to different subclasses of STLs, namely, helenalin acetate (**2**), a helenanolide-type pseudoguaianolide, and goyazensolide (**58**), a furanoheliangolide-type compound, were found to be the most active within the studied series. They displayed IC_{50} values of 0.7 and 0.6 μM, respectively, and thus interfered more potently with c-Myb activity than mexicanin I (**15**, 1.8 μM) and unesterified helenalin (**1**, 2.4 μM), both reported as potential c-Myb inhibitors in our previous study [17]. The IC_{50} values in the studied series of STLs ranged between 0.6 μM and >30 μM (which was the highest concentration tested, i.e. for compounds reported to show an IC_{50} above this cutoff value, no definite IC_{50} value could be determined). This latter category of compounds was thus considered inactive.

2.2. Cell viability measurements and relationships between biological activity data

Since STLs have long been known to cause cytotoxic cell damage, control measurements for cell viability in an MTS assay were carried out for all compounds with c-Myb IC_{50}s < 30 μM. The IC_{50} values for cell viability/cytotoxicity (Table 1) were generally significantly higher than those for c-Myb inhibition (e.g. 8.8 and 7.4 μM for goyazensolide **56** and helenalin acetate **2**), so that the observed inhibition of transcriptional activity was not solely due to unspecific cell damage.

However, since a linear correlation between the c-Myb inhibitory and the cytotoxicity data was found ($n = 60$, $R^2 = 0.57$; IC_{50} values >30 were arbitrarily set to 50; see Fig. 2A), there appears to be a direct relationship between these effects. Interestingly, a plot of the log selectivity index ($\log SI = pIC_{50}^{(c\text{-}Myb)} - pIC_{50}^{(MTS)}$) versus $pIC_{50}^{(c\text{-}Myb)}$ for compounds that allowed measurement of explicit IC_{50} values for both activities ($n = 16$) shows a strong positive correlation ($R^2_{linear} = 0.76$, see Fig. 2B) while there is no such correlation with $pIC_{50}^{(MTS)}$ ($R^2 = 0.03$; see Fig. 2C) indicating that selectivity increases as a function of c-Myb inhibitory potency rather than of basic cytotoxicity. This indicates that selective inhibition of the Myb-induced activation of the reporter gene can be differentiated from basic cytotoxicity so that it appears promising to investigate the chemical/structural reasons for selective c-Myb inhibition.

2.3. Structure–activity relationships

Potentially reactive structure elements such as α-methylene-γ-lactone (ML) and cyclopentenone (CP) or other conjugated enone (EN) groups are very common in natural sesquiterpene lactones and have been found essential for many biological activities of STLs [18–22] since they are known to inhibit the activity of many functional proteins [18,21]. It hence appears a very noteworthy initial observation that the presence of an ML group as such does not warrant c-Myb inhibitory activity. Several compounds possessing this structural feature were found essentially inactive in our assay. On the other hand, as has been found also in other SAR studies [19–22], the presence of at least one reactive structure element (CP, EN or ML) is required for activity since compounds **30** and **44** lacking any such feature are inactive. Thus, as already anticipated in our initial study [17], covalent protein modification is likely to represent the general mechanism of action.

On the other hand, we have already demonstrated in our previous study [17] that the reactive structure elements as found e.g. in helenalin (**1**) and its derivatives as well as in mexicanin I (**15**), namely, cyclopentene-2-one and α-methylene-γ-butyrolactone, are devoid of activity when tested as model chemicals on their own. Furthermore, we have also tested a 1:1 mixture of these two model chemicals and found it inactive so that a combined effect of the two reactive moieties independent of the sesquiterpene skeleton can definitely be ruled out. It thus becomes clear that the STL molecule bearing one or both partial structures in a chemical environment suitable to mediate interactions with the target by non-covalent binding is of great importance.

Comparing the activity of 11,13-dihydrohelenalin derivatives (**5**, **6**; only CP moiety) and a variety of 2,3-dihydropseudoguaianolides (**7**–**14**, **16**, **17**; only ML) with compounds of the helenalin and mexicanin I series (**1**–**4**, **15**; CP and ML), it can be concluded that the presence of both, an α,β-unsaturated ketone as well as a methylene lactone confers a much higher level of activity than the presence of either one alone.

The modulating influence of the STL skeleton on activity is nicely illustrated when comparing helenalin (**1**) and its acetate (**2**), isobutyrate (**3**) and methylbutyrates (mixture of 2-methylbutyrate and isovalerate, **4a** + **4b**). c-Myb induced reporter gene activity is maximally inhibited by the acetate **2** and activity decreases in the free alcohol **1** as well as the higher esters, being lowest in the methylbutyrates **4**. This effect related to the size of the ester group at C-6 is interesting to note since a similar decrease of activity is also observed for a compound with a larger ester group in the furanoheliangolide group (see below).

In the series of guaianolides and 4,5-secoguaianolides (xanthanolides) as well as the eudesmanolides, activity was moderate to low throughout. The highest activity among the guaianolides was observed with the simple guaianolide dehydrocostus lactone (**19**) which was more active than two compounds with an epoxide moiety and different mode of lactonization (**20**, **21**). Among the xanthanolides, 8-epixanthatin-1β,5β-epoxide (**23**) was the most (though only moderately) active derivative. In contrast to its monomeric xanthanolide congeners (**22**, **24**), compound **23** possesses an α,β-unsaturated keto group in addition to the methylene lactone moiety which apparently renders it somewhat more active. The two xanthanolide dimers **25** and **26** were inactive. Compound **26**, in addition to a further enone moiety, possesses the same reactive partial structures as **23**. It may hence be stated that its inactivity is probably related to its larger size. Among the eudesmanolides, isoalantolactone (**27**) was only slightly more active than its 2-hydroxy- and -acetoxy derivatives ivalin (**28**) and ivalin acetate (**30**) as well as its double bond isomer alantolactone (**31**) whereas some further compounds of this type (**32**,**33**) were inactive.

Within the relatively large and diverse group of germacranolides (**34**–**60**), considerable variability of activity (IC_{50} ranging from 0.63 to >30 μM) was observed. It is interesting to note that the most

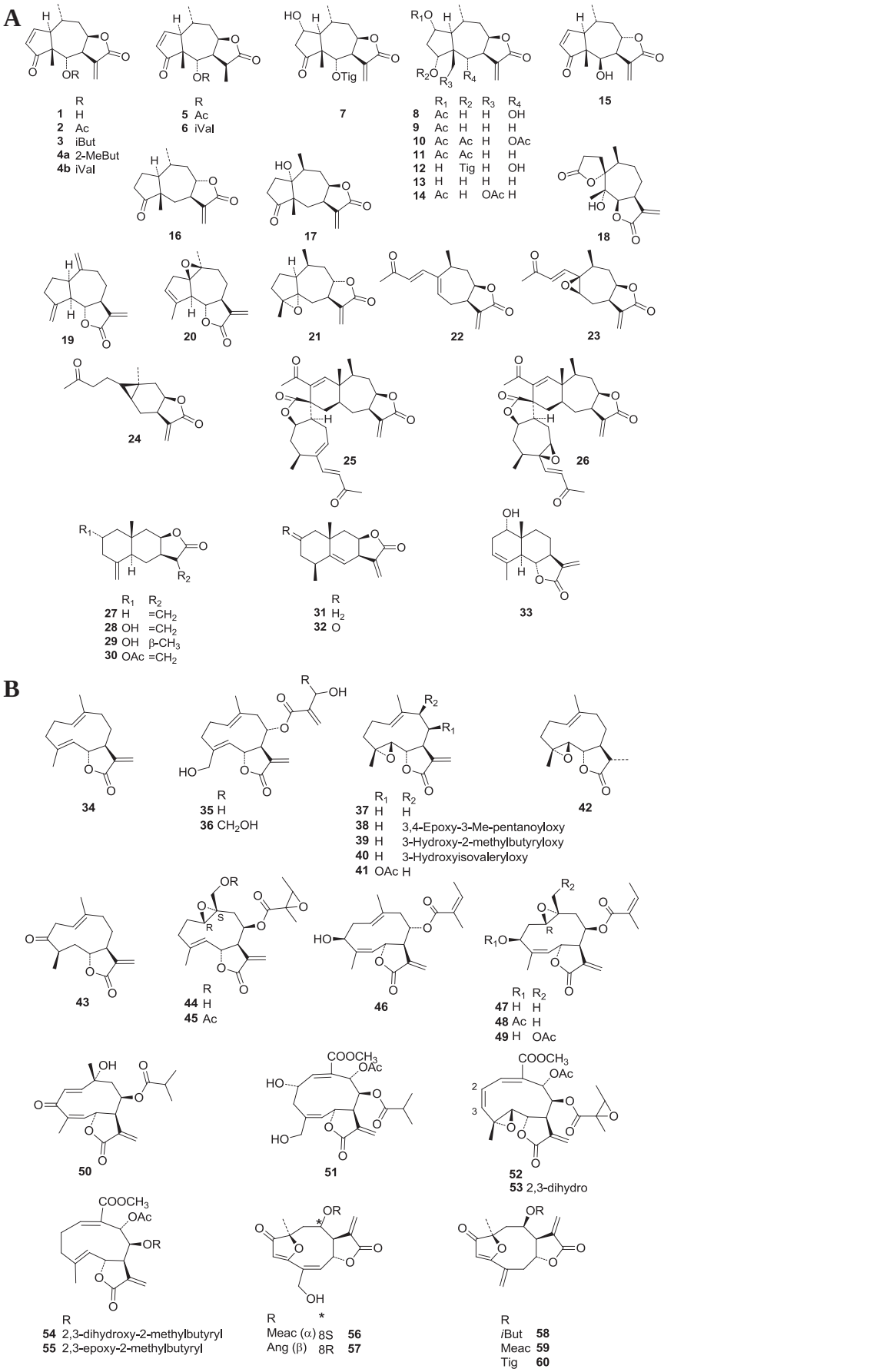

Fig. 1. A. Structures of tested STLs; pseudoguaianolides **1**–**18**, guaianolides **19**–**21**, xanthanolides (4,5-*seco*-guaianolides) **22**–**26**, eudesmanolides **27**–**33**. B. Structures of tested STLs of the germacranolide type (**34**–**60**).

Table 1
Biological activity data of the STL under study. c-Myb: Inhibition of c-Myb induced transcriptional activity; MTS: reduction of cell viability. All data for the c-Myb assay are based on three independent determinations. In case of the MTS assay, data reported as IC_{50} values are from triplicate determinations whereas data represented as cutoff values (>30, i.e. IC_{50} not reached up to 30 μM) were only reproduced once.

Compound		c-Myb		MTS	
		IC_{50} (μM)	(±SD)	IC_{50} (μM)	(±SD)
1	Helenalin	2.37	(0.39)	21.11	(2.63)
2	Helenalin acetate	0.71	(0.03)	7.34	(0.95)
3	Helenalin isobutyrate	2.54	(0.28)	>30	
4	Helenalin 2-methylbutyrate **4a** + -isovalerate **4b** (80:20)	7.19	(1.48)	>30	
5	11α,13-Dihydrohelenalin acetate	17.71	(2.36)	21.04	(2.43)
6	11α,13-Dihydrohelenalin isovalerate	16.63	(1.04)	>30	
7	Arnifolin	21.36	(4.90)	>30	
8	Chamissonolide	>30		>30	
9	6-Deoxychamissonolide	>30		>30	
10	4,6-Di-*O*-acetylchamissonolide	12.97	(4.05)	>30	
11	4-*O*-Acetyl-6-deoxychamissonolide	32.26	(4.31)	>30	
12	Deacetyl-4-*O*-tigloylchamissonolide	29.87	(1.31)	>30	
13	Deacetyl-6-deoxychamissonolide	>30		>30	
14	15-Acetoxy-6-deoxychamissonolide	>30		>30	
15	Mexicanin I	1.80	(0.06)	21.13	(2.19)
16	2,3-Dihydroaromaticin (=graveolide)	>30		>30	
17	Peruvin	>30		>30	
18	Psilostachyin A	>30		>30	
19	Dehydrocostuslactone	9.54	(0.46)	>30	
20	Arglabin	17.42	(1.99)	>30	
21	4α,5α-Epoxy-10α,14-dihydro-1-epi-inuviscolide	>30		>30	
22	8-Epixanthatin	>30		>30	
23	8-Epixanthatin-1β,5β-epoxide	13.22	(3.07)	>30	
24	Carabrone	>30		>30	
25	Pungiolide A	>30		>30	
26	Pungiolide B	>30		>30	
27	Isoalantolactone	19.23	(2.32)	>30	
28	Ivalin	25.48	(1.71)	>30	
29	11α,13-Dihydroivalin	>30		>30	
30	Ivalin acetate	22.08	(7.45)	>30	
31	Alantolactone	23.64	(6.16)	>30	
32	2-Oxoalantolactone	>30		>30	
33	Douglanin	>30		>30	
34	Costunolide	30.66	(4.79)	>30	
35	Onopordopicrin	13.73	(6.79)	>30	
36	Cnicin	17.92	(6.28)	>30	
37	Parthenolide	17.41	(1.49)	>30	
38	9β-Hydroxyparthenolide-3′,4′-epoxy-3′-methylpentanoate	13.43	(3.72)	22.25	(3.36)
39	9β-Hydroxyparthenolide-3′-hydroxy-2′-methylbutyrate	14.35	(6.45)	>30	
40	9β-Hydroxyparthenolide-3′-hydroxyisovalerate	17.77	(6.97)	>30	
41	Lipiferolide (=8β-hydroxyparthenolide acetate)	8.39	(1.14)	>30	
42	11β,13-Dihydroparthenolide	>30		>30	
43	Argolide	23.33	(2.78)	>30	
44	8β-Epoxyangeloyloxy-14-hydroxy-tithifolin	33.64	(4.81)	>30	
45	8β-Epoxyangeloyloxy-14-acetoxy-tithifolin	12.16	(4.11)	25.49	(7.25)
46	Nobilin	4.73	(1.40)	>30	
47	Leptocarpin	29.66	(7.55)	>30	
48	Leptocarpin acetate	>30		>30	
49	Rotundin	15.86	(1.01)	>30	
50	Tagitinin C	2.92	(1.08)	30.91	(10.93)
51	Melcanthin C	4.68	(1.64)	24.82	(4.36)
52	Leucanthin A	8.60	(5.45)	28.00	(7.24)
53	Enhydrin	2.95	(1.23)	7.49	(0.29)
54	Tetraludin A	21.37	(4.25)	>30	
55	Uvedalin	3.83	(1.22)	11.42	(4.19)
56	Goyazensolide	0.63	(0.19)	10.05	(3.96)
57	Budlein A	2.39	(0.25)	9.00	(2.96)
58	4,15-*iso*-Atriplicolide-8-*O*-isobutyrate	9.59	(2.19)	25.20	(3.21)
59	4,15-*iso*-Atriplicolide-8-*O*-methacrylate	2.21	(0.32)	10.38	(3.96)
60	4,15-*iso*-Atriplicolide-8-*O*-tiglate	1.57	(0.47)	12.07	(6.46)

active compound of the whole series, goyazensolide (**56**, IC_{50} = 0.63 μM) with a furanoheliangolide skeleton, also possesses an α,β,γ,δ-unsaturated keto structure besides the α-methylene-γ-lactone moiety so that also in this series, the presence of two potentially alkylating partial structures confers high activity. Also most other compounds of this series with additional enone moieties (**50**–**53**, **55**, **57**–**60**) displayed a relatively high level of activity. Quite interestingly, compounds **57**–**60**, quite similar to **56** in structure, were markedly less active. They differ from **56** in the configuration at C-8 and the nature of the ester side chain (**57**, **58**, **60**). Moreover, in **58**–**60**, the α,β,γ,δ-unsaturated carbonyl system has an exocyclic methylene carbon as potentially reactive site. Since **57**–**60** aligned very well with the structure of **56** (see next section) these subtle structural differences must be held responsible for the observed decrease in activity.

2.4. Computational studies on quantitative structure–activity relationships (QSAR)

Given the fact that compounds **2** and **56** are equally potent in spite of their rather different molecular scaffold, it is important to note that a comparison of their 3D structures and molecular surface reveals quite obvious similarities. An overlay of the two structures obtained by automatic flexible alignment based on pharmacophore features as implemented in the modeling package MOE [23] is shown in Fig. 3. From this graphical representation it becomes clear that the two most active compounds in the series share some very obvious similarities in terms of properties important for binding to a common hypothetical target. A graphical representation of common pharmacophoric features of **2** and **56** is depicted in Fig. 4. Overall, 6 of the 8 pharmacophore features in this model are identical in the two molecules. The only discrepancy is observed between the reactive β- and δ-carbons of the cyclopentenone moiety in **2** and the α,β,γ,δ-unsaturated ketone of **56**, respectively, which occupy different positions. These two reactive sites, however, are positioned in such a way that they could both react with the same SH group or other nucleophilic structure element of a common target protein. Another noteworthy point is that the ester side chains (acetate in **2** and methacrylate in **56**) adopt almost identical positions in this pharmacophoric alignment, so that the above-mentioned detrimental effect of the size of the ester groups on activity, observed with the helenalin- and furanoheliangolide series, could indeed be related to a steric problem for larger side chains to fit into a putative common binding site.

Based on this pharmacophore model and some related descriptors, a quantitative structure–activity relationship (QSAR) model for the whole series could be developed. To this end, all molecules in the series were aligned with the goyazensolide/helenalin acetate pair using the flexible alignment function of MOE as above. These aligned structures were analyzed for their agreement with the pharmacophore model by assessing the presence/absence of each of the 8 pharmacophoric features in each aligned structure. Thereby, a matrix of 8 indicator variables (1 in case of presence, 0 in case of absence of a feature; *F1*–*F8*; assignment see Fig. 4 and Table S2, Supplementary data) was generated for the 60 molecules. As further descriptors, the global alignment score (*S* [23], along with some global 3D descriptors as automatically calculated by MOE (for full list see Supplementary data)) were added to the descriptor matrix. This matrix was analyzed by partial least squares regression (PLS) as implemented in MOE for correlation with the biological activity data ($pIC_{50} = -\log IC_{50}$ [M]) using the QSAR module of MOE [23]. Before the regression analysis, the dataset was divided into a training set ($n = 40$) and a test set ($n = 20$) without consideration of the molecules' structure but in such a way that the range of biological activity data was covered by both sets in an even

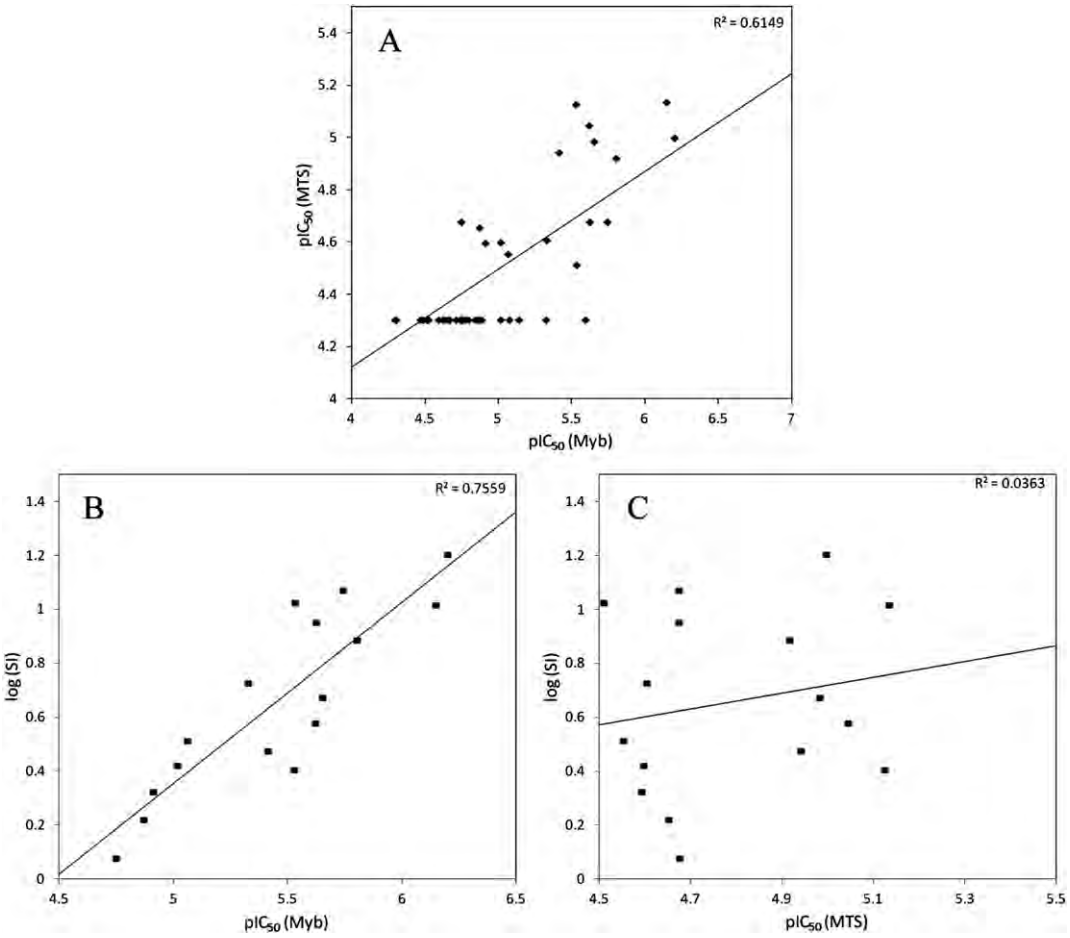

Fig. 2. A: Plot of pIC_{50} values for cell viability (MTS) vs. inhibition of c-Myb transcriptional activity (note that in case of compounds with $IC_{50} > 30$ in either assay, the IC_{50} value was arbitrarily set to 50). B: Plot of log SI [=pIC_{50}(c-Myb) − pIC_{50} (MTS)] vs. pIC_{50} (cMyb). C: Plot of log SI vs. pIC_{50} (MTS) for compounds ($n = 16$) that allowed explicit measurement of both IC_{50} values (≤30.0 μM).

manner. In the following PLS regression analyses performed with the 40 training molecules, the 8 pharmacophore descriptors (*F1*–*F8*) used on their own yielded a squared correlation coefficient (R^2) of 0.65. This value increased to 0.73 when the global alignment score *S* was added as further descriptor. Addition of two further descriptors of 3D structure, namely, ASA^+ and ASA^-, encoding each molecule's accessible surface area covered by atoms with positive and negative partial charges, respectively, led to a further increase of R^2 to 0.84 and a cross-validated correlation coefficient Q^2 of 0.70. Subsequent elimination of variables yielding only statistically insignificant contributions to the overall regression led to a QSAR model described by the following multiple linear regression equation:

$$\begin{aligned} pIC_{50} = {} & 5.885(\pm 1.029) - 0.588(\pm 0.109)S + 0.255(\pm 0.084)F1 \\ & + 0.451(\pm 0.088)F2 - 0.269(\pm 0.089)F4 \\ & + 0.409(\pm 0.088)F6 - 0.574(\pm 0.142)ASA^+ \\ & + 0.242(\pm 0.168)ASA^- \end{aligned} \quad (1)$$

(R^2 = 0.83, RMSE = 0.21; Q^2 (leave-one-out cross validation) = 0.72, RMSE = 0.28; Data were standardized to unit variance.)

The model represented by equation (1) was then used to predict the activity for the 20 test set molecules yielding a squared correlation coefficient for the predictions vs. the experimental data of P^2 = 0.65 (RMS error of predictions = 0.29) which confirms the underlying structure–activity relationship's applicability to external predictions. A plot of the experimental vs. calculated activity data is shown in Fig. 5.

Of the four pharmacophore descriptors, three encode for the presence of the three potentially reactive structure elements (i.e. reactive carbons of methylene lactone (*F1*), cyclopentenone (*F2*) and α,β,γ,δ-unsaturated ketone (*F6*), respectively), which is in agreement with the importance of these structural features already discussed above. Quite noteworthy, indicator variables encoding only for the presence/absence of the various potentially reactive structure elements in the molecules (i.e. without taking into account the fit with the pharmacophore model, see Table S2, Supplementary data) as previously used in QSARs for cytotoxic activity of STLs [19,20], when combined with *S*, ASA^+ and ASA^-, yielded a much inferior correlation (R^2 = 0.67, Q^2 = 0.42). This finding clearly underlines the relevance of the geometrical arrangement of the Michael acceptor sites.

Feature *F4* represents the hydrogen bond acceptor property associated with the carbonyl oxygen activating *F1* and *F6*. This feature, somewhat surprisingly, shows a negative regression coefficient in the QSAR equation which can, however, be explained by the fact that several compounds with low or no activity have a potential acceptor atom at this site which is not part of a reactive structure element. Hence, the occurrence of this feature without simultaneous presence of the conjugated reactive site yields a negative impact on activity. The alignment score *S* expresses each molecule's potential to adopt a conformation in which

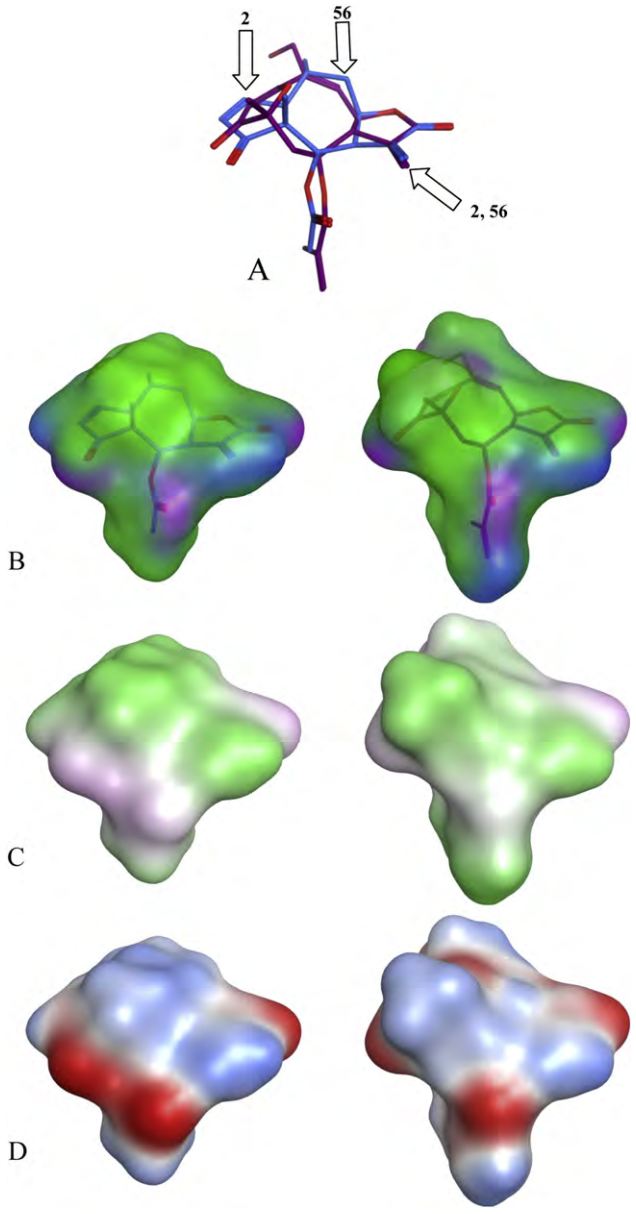

Fig. 3. Comparison of the molecular structures of helenalin acetate (**2**) and goyazensolide (**56**), the most active compounds in the present series. A: superposition as obtained by flexible alignment based on pharmacophoric atom properties using MOE [23], blue: **2**; violet: **56**; Arrows denote the position of Michael acceptor sites. B–D: Comparison of molecular surface representations (left: **2**; right: **56**) color-coded by: B: active lone pair/hydrophobic features (blue/pink: polar/hydrogen bonding propensity, green: hydrophobic), C: lipophilicity (green: lipophilic, white: neutral, pink: hydrophilic), D: electrostatic potential (red: negative, blue: positive). (For interpretation of the references to color in this figure legend, the reader is referred to the web version of this article.)

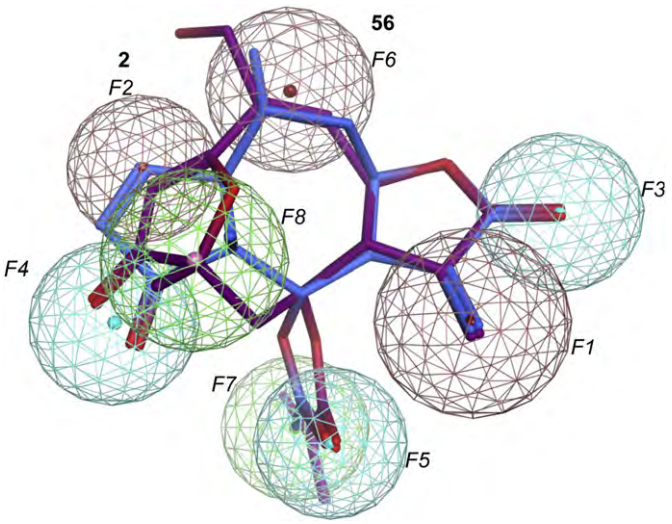

Fig. 4. Common pharmacophore features of helenalin acetate (**2**, blue carbons) and goyazensolide (**56**, violet carbons). Pharmacophore spheres: blue: hydrogen bond acceptor; green: hydrophobe; red: reactive carbon of α,β-(**2**) or α,β,γ,δ-(**56**) unsaturated keto carbonyl (labeled according to compound) and of α-methylene-γ-lactone structures. Numbering of features *F1–F8* as used in the QSAR study. (For interpretation of the references to color in this figure legend, the reader is referred to the web version of this article.)

pharmacophoric structure elements are oriented in a similar way as in **2** and **56**. A more negative value of *S* means better fit (higher structural similarity in terms of pharmacophoric properties and/or a lower strain energy associated with the alignment) so that the negative regression coefficient of this descriptor is in agreement with the general pharmacophore hypothesis underlying these considerations. The statistically significant contributions of these descriptors to the QSAR model underline the relevance of the pharmacophore hypothesis for **2** and **56**. The information content encoded in these descriptors already explains about 73% of the total variance in the biological data. It is further complemented by the ASA descriptors which encode in a more global way the overall properties of the molecules in terms of charge distribution on their molecular surface. Here, the positive contribution of ASA^- (due in this series mainly to oxygen atoms, i.e. potential H-bond acceptors) indicates that in general a larger fraction of negative partial charge has an enhancing effect on activity while the positively charged surface encoded by ASA^+ has a detrimental effect.

This QSAR model has the advantage of being quite straightforward to interpret due to the simplicity of the descriptors and their direct relation to the pharmacophore model. Although derived from a relatively small range of activity data, the model is capable of describing about 83% of the variance of activity within the current

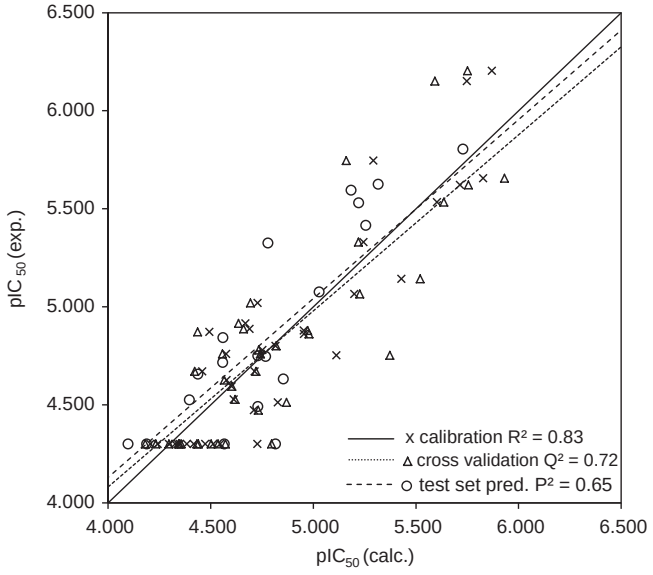

Fig. 5. Plot of experimental versus calculated pIC_{50} values as obtained from the QSAR model represented by equation (1).

dataset and also allows predictions for further STLs with a reasonable degree of certainty.

Together with the underlying pharmacophore model, this QSAR can now be used for ligand-based screening of virtual compound libraries such as our in-house database of over 2000 sesquiterpene lactones, which will possibly yield hits of other subclasses possessing similarly high or even higher activity. The applicability of the pharmacophore model as a template for virtual screening of other structural classes will also be tested.

2.5. Conclusion

Our finding that some STLs are able to interfere potently with the transcriptional activity of c-Myb represents a novel mechanistic aspect with respect to the often reported potential of such compounds as anti-cancer leads (see e.g. literature cited in Refs. [17,18,21]; for recent reviews see Refs. [24,25]).

The present data show that STLs of a great structural diversity demonstrate inhibitory activity on c-Myb-dependent gene expression and might thus be useful as lead structures for new antileukemic therapies. The potency of such compounds appears to be more or less independent of the underlying type of sesquiterpene skeleton since the most active compounds found so far are helenalin acetate, a pseudoguaianolide, and goyazensolide, a germacranolide of the furanoheliangolide subgroup. The finding that these two compounds show conspicuous similarity in their three-dimensional molecular structure indicates that the observed high level of activity is due to specific binding to a common – yet unknown – binding site. This hypothesis is also corroborated by the finding that a common QSAR could be derived for all molecules of the series which is based mainly on descriptors derived directly from the pharmacophore model.

Based on the presented structure–activity relationships, the search for further compounds with similarly high or even higher activity can be carried on to larger libraries of natural products or non-natural analogs.

3. Experimental section

3.1. Bioassays

HD11-C3 is a myelomonocytic chicken cell line expressing doxycyclin-inducible chicken c-Myb protein. HD11-C3-GFP1 is a subclone of HD11-C3 stably transfected with a reporter gene carrying the enhancer and promoter of the Myb-inducible *mim-1* gene [26,27] in front of the coding region of eGFP [17].

3.1.1. Effect of test compounds on Myb-dependent transcriptional activity (GFP-assay)

To determine the effect of sesquiterpene lactones of the Myb-dependent activation of the reporter gene, the cells were treated with 1 μg/ml doxycyclin and the STL at various concentrations (typically 4) above and below the IC_{50}. As negative control, cells were treated with doxycyclin only. The cells were harvested after 24 h and measurement of their fluorescence intensity (excitation wave length 485 nm, emission wave length 530 nm) was performed with a fluorescence microplate reader (Mithras LB 940, Berthold Technologies). Each compound was tested three times independently. To compensate for background fluorescence, caused by a low level of basal expression of the *mim-1*/eGFP construct, the fluorescence of untreated cells was also measured and subtracted from each value measured for the treated cells. The reported IC_{50} values were obtained by linear interpolation between the averaged fluorescence values obtained with the two closest concentrations above and below the IC_{50} value.

3.1.2. Effect of test compounds on cell viability

To exclude a general cytotoxic effect as mere cause for the inhibitory effect, cell viability was determined in MTS assays. Cells were treated under the same conditions as reported above and incubated with the STL (same concentrations as above) for 24 h. After that, 20 μl of MTS solution (CellTiter 96® Aqueous One Solution, Promega) were added to each well and incubated for 1 h. Untreated cells with MTS solution were used as control; growth medium with the tested STL and MTS solution was used for the determination of background absorbance. The absorbance at 492 nm was measured with a microplate photometer (MPP 4008, Mikrotek). Compounds with an inhibitory activity in the GFP-assay were tested three times independently. Cell viability determinations for compounds with an $IC_{50} > 30$ μM in the GFP-assay were only reproduced once. IC_{50} values were determined by linear interpolation between the averaged absorbance values obtained with the two closest concentrations above and below the IC_{50} value.

3.2. Tested sesquiterpene lactones

For the origin of the tested compounds see Table S1, Supplementary data. The identity and purity of all compounds were assessed by ^{1}H NMR (see Table S1 and Fig. S1–S60, Supplementary data, for estimated purity and ^{1}H NMR spectra, respectively). Stock solutions (10 mM) were prepared in DMSO, which were diluted with growth medium to the final specified concentrations.

3.3. Computational methods

Three-dimensional molecular models of all compounds were generated with MOE [23] using the MMFF94x force field. A low-mode dynamics conformational search was performed for each compound (default settings of MOE) and the resulting conformers with lowest force field energy (within an energy window of 3 kcal/mol above the lowest minimum) were kept for further investigations.

The structural comparison of compounds **2** and **56** (Figs. 3 and 4) was carried out using the flexible alignment function of MOE [23] with standard settings. The pharmacophore model was generated with the MOE pharmacophore query editor. The query was calibrated in such a way that compounds **2** and **56** were found in a variety of molecular databases.

For the QSAR analysis, each molecule was aligned with the dual alignment of **2** and **56** (see above) using the same settings. Each superposed structure was then visually matched with the pharmacophore model (see above) and binary indicator variables were generated which were assigned a value of 1 if the compound possessed a particular feature and 0 otherwise. Thus, 8 indicator variables were obtained. *F1*: Michael acceptor carbon corresponding to reactive β-exomethylene of methylene lactone group, *F2*: Michael acceptor carbon corresponding to reactive β-position of cyclopentenone of **2**, *F3*: H-bond acceptor corresponding to carbonyl oxygen of methylene lactone group, *F4*: H-bond acceptor corresponding to carbonyl oxygen of cyclopentenone (**2**) and furanone (**56**) moiety; *F5*: H-bond acceptor corresponding to ester carbonyl moiety; *F6*: Michael acceptor carbon corresponding to the reactive δ-position of α,β,γ,δ-unsaturated ketone structure in **56**; note that this feature was positioned in such a way that it also accommodates the related structure element of compounds **58**–**60**. *F7*: hydrophobic feature corresponding to acetyl and methacryloyl moieties in **2** and **56**, *F8*: hydrophobic feature corresponding to CH_3-15 in **2** and CH_3-14 in **56**. These indicators were used as QSAR descriptors together with the global alignment score *S*, a measure for the fit of the molecular structure to the alignment of **2** and **56**, and several further internal 3D descriptors. A full list of descriptors taken into consideration is reported in Table S2, Supplementary data. The IC_{50} data for the

inhibition of c-Myb transcriptional activity, expressed on the molar scale, were converted to negative decadic logarithms (pIC_{50}); values for compounds with $IC_{50} > 30$ μM were arbitrarily set to 50 μM. The compounds were divided into a training set ($n = 40$) and a test set ($n = 20$) irrespective of their chemical structure but in such a way that both sets covered evenly the range of biological activities. Partial least squares (PLS) regression as implemented in MOE [23] was used to analyze the correlation of the descriptor matrix of the training set with biological activity, starting with the pharmacophore descriptors (*F1*–*F8*, *S*). After elimination of variables with low statistical relevance, descriptors *F1*, *F2*, *F4*, *F6* and *S* yielded a PLS regression with $R^2 = 0.67$ and $Q^2 = 0.58$ for leave-one-out cross validation. Combinations of this model with 1 and 2 further descriptors in an attempt to maximize the correlation and internal predictivity revealed significant influences of ASA^+ and ASA^- (standard internal 3D descriptors calculated by MOE [23]), which then yielded the final model used to predict the activities of the test set. This model is presented in Fig. 5 and discussed in the text. The full descriptor matrix used for this model is reported in Table S3, Supplementary data.

As a final test for the validity of the model, a series of three scramble tests were performed. The activity data of the training set were randomly re-assigned to the compounds and the PLS regression repeated with the same descriptors. The resulting regression equations were also used to predict the activity of the test set whose data were not scrambled. Neither significant correlations nor any internal or external predictivity was found with these scrambled data ($R^2 = 0.21/0.06/0.22$, $Q^2 = 0.0006/0.14/0.006$ and P^2(test set) = 0.009/0.13/0.06 for three scramble tests), confirming that the correlations and predictions for the true data were not due to chance correlation.

Acknowledgments

Financial support from Deutsche José Carreras Leukämie-Stiftung is most gratefully acknowledged. F.B. Da Costa acknowledges FAPESP, CAPES and CNPq for financial support. Thanks are due to Dr. A. Gökbulut (Ankara, Turkey) for isolating compounds **16**, **21**, **40**–**42** and to Lara Zimmermann (Florianópolis, Brazil) for isolating compounds **20**, **45** and **48**, during internships at IPBP, Münster. We also thank N. Kretschmer (Graz, Austria) for isolating compound **60**. Furthermore, a variety of compounds (see Table S1, Supplementary data) were kindly provided by G. Willuhn (formerly University of Düsseldorf, Germany) and N.H. Fischer (formerly University of Oxford, Ms, USA) for which we express our special gratitude.

Appendix A. Supplementary data

Supplementary data related to this article can be found at http://dx.doi.org/10.1016/j.ejmech.2013.02.018.

References

[1] K. Weston, Myb proteins in life, death and differentiation, Curr. Opin. Genet. Dev. 8 (1998) 76–81.
[2] J.S. Lipsick, D.M. Wang, Transformation by v-Myb, Oncogene 18 (1999) 3047–3055.
[3] I.-H. Oh, E.P. Reddy, The *myb* gene family in cell growth, differentiation and apoptosis, Oncogene 18 (1999) 3017–3033.
[4] R.J. Ramsay, T.J. Gonda, Myb function in normal and cancer cells, Nat. Rev. Cancer 8 (2008) 523–534.
[5] M.L. Mucenski, K. McLain, A.B. Kier, S.H. Swerdlow, C.M. Schreiner, T.A. Miller, D.W. Pietryga, W.J. Scott Jr., S.S. Potter, A functional c-*myb* gene is required for normal murine fetal hepatic hematopoiesis, Cell 65 (1991) 677–689.
[6] N. Emambokus, A. Vegiopoulos, B. Harman, E. Jenkinson, G. Anderson, J. Frampton, Progression through key stages of haemopoiesis is dependent on distinct threshold levels of c-Myb, EMBO J. 22 (2003) 4478–4488.
[7] T.P. Bender, C.S. Kremer, M. Kraus, T. Buch, K. Rajewsky, Critical functions for c-Myb at three checkpoints during thymocyte development, Nat. Immunol. 5 (2004) 721–729.
[8] M.R. Carpinelli, D.J. Hilton, D. Metcalf, J.L. Antonchuk, C.D. Hyland, S.L. Mifsud, L. Di Rago, A.A. Hilton, T.A. Willson, A.W. Roberts, R.G. Ramsay, N.A. Nicola, W.S. Alexander, Suppressor screen in Mpl−/− mice: c-Myb mutation causes supraphysiological production of platelets in the absence of thrombopoietin signaling, Proc. Natl. Acad. Sci. USA 101 (2004) 6553–6558.
[9] M.L. Sandberg, S.E. Sutton, M.T. Pletcher, T. Wiltshire, L.M. Tarantino, J.B. Hogenesch, M.P. Cooke, c-Myb and p300 regulate hematopoietic stem cell proliferation and differentiation, Dev. Cell 8 (2005) 153–166.
[10] M.D. Thomas, C.S. Kremer, K.S. Ravichandran, K. Rajewsky, T.P. Bender, c-Myb is critical for B cell development and maintenance of follicular B cells, Immunity 23 (2005) 275–286.
[11] J. Sitzmann, K. Noben-Trauth, K.-H. Klempnauer, Expression of mouse c-myb during embryonic development, Oncogene 11 (1995) 2273–2279.
[12] J. Malaterre, M. Carpinelli, M. Ernst, W. Alexander, M. Cooke, S. Sutton, S. Dworkin, J.K. Heath, J. Frampton, G. McArthur, H. Clevers, D. Hilton, T. Mantamadiotis, R.G. Ramsay, c-Myb is required for progenitor cell homeostasis in colonic crypts, Proc. Natl. Acad. Sci. USA 104 (2007) 3829–3834.
[13] J.J. Rushton, L.M. Davis, W. Lei, X. Mo, A. Leutz, S.A. Ness, Distinct changes in gene expression induced by A-Myb, B-Myb and c-Myb proteins, Oncogene 22 (2003) 308–313.
[14] G. Lang, J.R. White, M.J. Argent-Katwala, C.G. Allinson, K. Weston, Myb proteins regulate the expression of diverse target genes, Oncogene 24 (2005) 1375–1384.
[15] F. Liu, W. Lei, J.P. O'Rourke, S.A. Ness, Oncogenic mutations cause dramatic, qualitative changes in the transcriptional activity of c-Myb, Oncogene 2 (2006) 5795–5805.
[16] T. Berge, V. Matre, E.M. Brendeford, T. Saether, B. Lüscher, O.S. Gabrielsen, Revisiting a selection of target genes for the hematopoietic transcription factor c-Myb using chromatin immunoprecipitation and c-Myb knockdown, Blood Cells Mol. Dis. 39 (2007) 278–286.
[17] T. Bujnicki, C. Wilczek, C. Schomburg, F. Feldmann, P. Schlenke, C. Müller-Tidow, T.J. Schmidt, K.-H. Klempnauer, Inhibition of Myb-dependent gene expression by the sesquiterpene lactone mexicanin-I, Leukemia 26 (2012) 615–622.
[18] T.J. Schmidt, Toxic activities of sesquiterpene lactones – structural and biochemical aspects, Curr. Org. Chem. 3 (1999) 577–605.
[19] T.J. Schmidt, Quantitative structure–cytotoxicity relationships within a series of helenanolide type sesquiterpene lactones. (Helenanolide type sesquiterpene lactones, IV, Pharm. Pharmacol. Lett. 9 (1999) 9–13.
[20] T.J. Schmidt, J. Heilmann, Quantitative structure–cytotoxicity relationships of sesquiterpene lactones derived from partial charge (Q)-based fractional accessible surface area descriptors (Q_frASAs), Quant. Struct.–Act. Relat. (QSAR) 21 (2002) 276–287.
[21] T.J. Schmidt, Structure–activity relationships of sesquiterpene lactones, in: Atta-ur-Rahman (Ed.), Studies in Natural Products Chemistry, vol. 33, Elsevier, Amsterdam, 2006, pp. 309–392.
[22] T.J. Schmidt, A.M.M. Nour, S.A. Khalid, M. Kaiser, R. Brun, Quantitative structure–antiprotozoal activity relationships of sesquiterpene lactones, Molecules 14 (2009) 2062–2076.
[23] Chemical Computing Group, Molecular Operating Environment (MOE). rel. 2011.10, Chemical Computing Group Inc, 1010 Sherbooke St. West, Suite #910, Montreal, QC, Canada, H3A 2R7, 2011.
[24] I. Merfort, Perspectives on sesquiterpene lactones in inflammation and cancer, Curr. Drug Targets 12 (2011) 1560–1573.
[25] M.R.O. Kreuger, S. Grootjans, M.W. Biavatti, P. Vandenabeele, K. D'Herde, Sesquiterpene lactones as drugs with multiple targets in cancer treatment: focus on parthenolide, Anti-cancer Drugs 23 (2012) 883–896.
[26] O. Chayka, J. Kintscher, D. Braas, K.-H. Klempnauer, v-Myb mediates cooperation of a cell-specific enhancer with the *mim*-1 promoter, Mol. Cell. Biol. 25 (2005) 499–511.
[27] C. Wilczek, O. Chayka, A. Plachetka, K.-H. Klempnauer, Myb-induced chromatin remodeling at a dual enhancer/promoter element involves non-coding RNA transcription and is disrupted by oncogenic mutations of v-myb, J. Biol. Chem. 284 (2009) 35314–35324.